Crystal-field excitations in multiferroic TbMnO3 by Mn L3 and O K resonant inelastic X-ray scattering

Jiatai Feng, Amélie Juhin, Renaud Delaunay, Romain Jarrier, Nicolas Jaouen, Alessandro Nicolaou, Ryan Sinclair, Haidong Zhou, Jean-Michel Mariot, Sorin G Chiuzbăian

Crystal-field excitations in multiferroic $TbMnO_3$ by Mn L_3 and O K resonant inelastic X-ray scattering

Jiatai Feng, Amélie Juhin, Renaud Delaunay, Romain Jarrier, Nicolas Jaouen, Alessandro Nicolaou, Ryan Sinclair, Haidong Zhou, Jean-Michel Mariot, and Sorin G. Chiuzbăian

Citation: Journal of Applied Physics **122**, 194101 (2017);
View online: https://doi.org/10.1063/1.4990683
View Table of Contents: http://aip.scitation.org/toc/jap/122/19
Published by the American Institute of Physics

JOURNAL OF APPLIED PHYSICS **122**, 194101 (2017)

Crystal-field excitations in multiferroic $TbMnO_3$ by Mn L_3 and O K resonant inelastic X-ray scattering

Jiatai Feng,[1] Amélie Juhin,[2] Renaud Delaunay,[1,3] Romain Jarrier,[1,3] Nicolas Jaouen,[3] Alessandro Nicolaou,[3] Ryan Sinclair,[4] Haidong Zhou,[4] Jean-Michel Mariot,[1,3] and Sorin G. Chiuzbăian[1,3,a)]

[1]*Sorbonne Universités, UPMC Univ Paris 06, CNRS, Laboratoire de Chimie Physique–Matière et Rayonnement (UMR 7614), 4 place Jussieu, 75252 Paris Cedex 05, France*
[2]*Sorbonne Universités, UPMC Univ Paris 06, CNRS, IRD, MNHN, Institut de Minéralogie, de Physique des Matériaux et de Cosmochimie (UMR 7590), 4 place Jussieu, 75252 Paris Cedex 05, France*
[3]*Synchrotron SOLEIL, L'Orme des Merisiers, Saint-Aubin, B. P. 48, 91192 Gif-sur-Yvette, France*
[4]*Department of Physics and Astronomy, Experimental Condensed Matter Physics, University of Tennessee, 407A Nielsen Physics Building, Knoxville, Tennessee 37996-1200, USA*

(Received 16 June 2017; accepted 28 October 2017; published online 16 November 2017)

d–d excitations in multiferroic $TbMnO_3$ have been investigated by X-ray absorption spectroscopy and resonant inelastic X-ray scattering at the Mn $L_{3,2}$ and O K edges. Confrontation between experimental data and multiplet crystal-field calculations performed for Mn^{3+} ions in D_{4h} symmetry has enabled us to identify the origin of the observed excitations and has provided reliable manganese crystal-field parameters that enter the description of the antisymmetric exchange interaction responsible for the multiferroicity in this compound. *Published by AIP Publishing.*
https://doi.org/10.1063/1.4990683

I. INTRODUCTION

Magnetic ferroelectric materials, usually referred to as multiferroics, are presently one of the most actively studied fields in solid state physics.[1,2] Interest in multiferroics arises from the prospect of controlling magnetic polarization, **M**, by means of an applied electric field or, inversely, by using a magnetic field to switch electrical polarization **P**. The interdependence of **M** and **P** is clearly inspiring for applications in the field of memory devices and spintronics. Two main classes of multiferroics have been identified.[2,3] For type-I multiferroics, the ferroelectricity is driven by structural effects generally described as ionic displacements starting from a centrosymmetric structure. $BiFeO_3$ is a renowned example with a large **P**, on the order of 100 μC cm^{-2}. In the case of type-II multiferroics, the electric polarization arises specifically as a consequence of the breaking of the magnetic order inversion symmetry. One of the most prominent examples in this class is $TbMnO_3$[4–6] where a spiral magnetic structure, present below 28 K, results in an electric polarization ascribed to electronic charge/spin currents.[7,8] When the inversion symmetry of the magnetic structure is broken, ferroelectric polarization can develop. While the polarization **P** obtained for $TbMnO_3$ is relatively small, about 0.06 μC cm^{-2}, the displayed magnetoelectric coupling between **M** and **P** is particularly strong.[4]

In more recent studies on $TbMnO_3$, Wilkins *et al.*[9] have produced evidence in favor of two noncollinear magnetic structures below 28 K, while Walker *et al.* have indicated that ionic displacements on a femtometer scale are present when a magnetic field is applied.[10,11] Therefore, it is likely that the origin of ferroelectric polarization in $TbMnO_3$ is very complex and may well involve some aspects of both type-II and type-I materials. A crucial ingredient for answering this question is the value of the crystal field (CF) acting on the transition-metal sites. For instance, the knowledge of the CF can be used as benchmark for the electronic structure calculations in both types of multiferroics,[12,13] as it includes the effective on-site electronic correlations. Furthermore, the single ion magnetic anisotropy of Mn^{3+} ions depends explicitly on the 3*d* CF splittings[14,15] and plays a pivotal role in the antisymmetric exchange interaction which drives the type-II multiferroicity. This paper deals with the quantification of the CF on Mn sites in $TbMnO_3$.

In an ideal ABO_3 perovskite structure, corner-sharing BO_6 octahedra are stacked along equivalent [1 0 0] directions, where A is a large radius cation (e.g., alkaline earths, some 4*d* transition metals, and rare earths) and B is a small radius 3*d* transition-metal cation. The A cations are located at the center of the cuboctahedral void created by the assembly of eight BO_6 octahedra. In the rare-earth manganites, A and B are rare earth and manganese trivalent ions (Mn^{3+}), respectively. The strain due to the large mismatch between the volume of the rare-earth ion and that of the void between the MnO_6 octahedra is at the origin of the departure from the ideal cubic perovskite structure in rare-earth manganites: the so-called $GdFeO_3$ orthorhombic distortion, i.e., a symmetry lowering from the $Pm\bar{3}m$ to the $Pbnm$ space group due to a cooperative rotation of the MnO_6 octahedra along the orthorhombic [0 1 0] and [0 0 1] directions [see Figs. 1(a) and 1(b)]. This distortion alters the Mn–O–Mn bond angle from 180° in the undistorted structure to $\approx$150°, a much smaller value. The octahedral environment of the Mn^{3+} ($3d^4$) ion splits the 3*d* atomic level into t_{2g} and e_g orbitals, leading to the high-spin $t_{2g}^3 e_g^1$ configuration. According to the Jahn–Teller theorem, the degeneracy of these orbitals should be lifted by distorting the BO_6

a)Author to whom correspondence should be addressed: gheorghe.chiuzbaian@upmc.fr

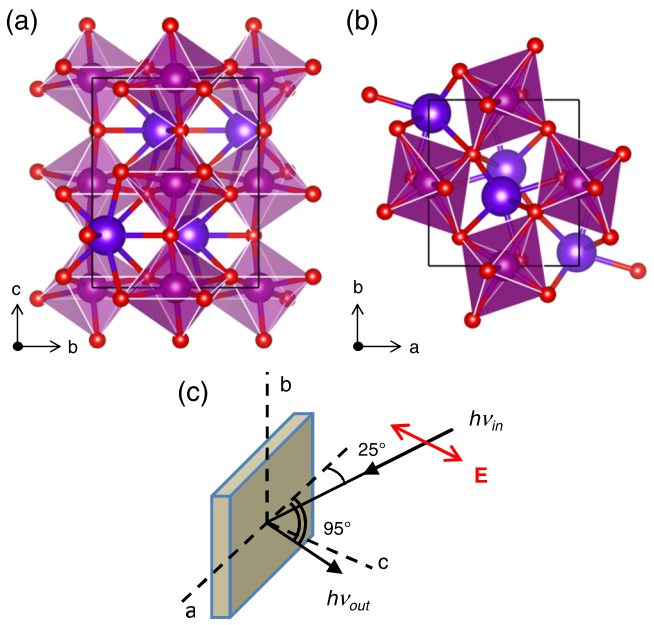

FIG. 1. $TbMnO_3$ crystalline structure and experimental arrangement. (a) and (b) Tilt of the MnO_6 octahedra as viewed facing the **a** and **c** axis, respectively. (c) Layout of the scattering geometry used in the RIXS measurements. **E** denotes the electric vector of the incoming LH polarized light (π polarization).

octahedra.[16] In the case of $TbMnO_3$, the MnO_6 octahedra are elongated along one O–Mn–O direction (Mn–O bond length of 2.25 Å), the bond lengths in the plane perpendicular to this direction being 1.89 and 1.95 Å; all O–Mn–O angles are conserved.[17]

Due to the presence of an inversion center in the crystal structure, $TbMnO_3$ is paraelectric at room temperature. Upon lowering the temperature, $TbMnO_3$ undergoes three magnetic phase transitions. The first two are related to spin ordering of the Mn^{3+} ions; the third is related to the Tb^{3+} ions. An A-type antiferromagnetic order sets in at $T_{N_1} \approx 41$ K as an incommensurate sinusoidal order; then, at $T_{N_2} \approx 28$ K, a transversally modulated spiral structure appears and gives birth to a ferroelectric polarization along the **c** axis;[4,6] finally, at ≈7 K, the magnetic moments of the Tb^{3+} ions order antiferromagnetically along the **a** axis.[5,18]

Here, we present high-resolution resonant inelastic X-ray scattering (RIXS) measurements on $TbMnO_3$ performed with soft X-rays at the Mn L_3 and O K edges. RIXS is ideally suited for observing neutral low-energy excitations[19] and charge transfer (CT) between a transition metal and a ligand. The dipole selection rules in both the excitation and the relaxation channels make RIXS uniquely adapted to measuring d–d excitations. Hence, importantly here, it provides a precise means of determining the CF by confronting CF multiplet calculations with experimental data.

Experimental conditions are reported in Sec. II. Section III introduces the framework of the CF multiplet calculations for both XAS and RIXS. The comparison between calculations and measurements is given in Sec. IV, followed by a more general discussion (Sec. V). Conclusions are drawn in Sec. VI.

II. EXPERIMENTAL

$TbMnO_3$ single crystals were grown in an Ar atmosphere using the floating zone technique.[20] The crystalline structure of the sample was checked by X-ray diffraction and its orientation determined from Laue X-ray diffraction patterns. The sample was bonded to a holder using a conductive epoxy resin such that its surface normal was oriented parallel to the (0 0 1) plane. The surface of the sample was scraped with a diamond file in the load-lock chamber under a pressure of 2×10^{-7} mbar and immediately transferred to the analysis chamber under a pressure lower than 5×10^{-9} mbar. As the sample is scraped in a vertical position, the presence of randomly oriented crystallites at the surface that might contribute to the XAS/RIXS signals is unlikely.

The experiments were carried out at the SEXTANTS beamline[21] of Synchrotron SOLEIL (France). A He flow cryostat was used to lower the sample temperature. XAS spectra were recorded in total electron yield (TEY) mode by measuring the sample drain current. The RIXS measurements were performed with the AERHA spectrometer.[22] The beam, tuned to a specific resonance with an energy $h\nu_{in}$, impinged on the sample at 25° grazing incidence. The energy distribution of the scattered photons, $h\nu_{out}$, was analyzed using a 1800 lines/mm diffraction grating and recorded with a charge-coupled device cooled to –110 °C. Thanks to the specific design of the AERHA spectrometer, the energy resolution can be varied to get a satisfactory compromise between resolving power and counting rate. In the present experiment, the overall energy resolution of the RIXS data was 170 meV at the Mn $2p_{3/2}$–$3d$ resonance (L_3 edge ∼640 eV) and 140 meV at the O $1s$–$2p$ threshold (K edge ∼530 eV). The values of the beamline slits were such that $h\nu_{in}$ contributed a broadening of 140 meV at Mn L_3 and 100 meV at O K edges.

III. XAS AND RIXS CALCULATIONS

Semi-empirical CF multiplet calculations based on the Cowan–Butler–Thole code[23,24] were performed to match both the experimental Mn $L_{3,2}$ XAS and L_3 RIXS spectra with the *same* set of parameters. A detailed account of the methodology used in the present calculations is given in Ref. 25. CT effects were not taken into account in order to reduce the number of parameters involved. In the vicinity of the $L_{3,2}$ XAS white lines, the spectral features are only slightly affected by CT effects.[26] In the case of the L_3 RIXS spectra, the inclusion of CT shifts spectral weight to higher transferred energies, ($h\nu_{in} - h\nu_{out}$), and gives rise to CT spectral features, but *does not* alter the position of the CF multiplets.[25] A reduction factor of 65% is applied to the *ab initio* Hartree–Fock values of the direct (F^k) and exchange (G^k) Slater–Condon integrals to take into account the expansion of the electron cloud in the solid compared to the atomic distribution. The computed spectra were broadened by the intrinsic and experimental effects. The XAS final state has a Lorentzian broadening determined by the $2p$ core-hole lifetime: ≈0.20 eV and ≈0.32 eV for Mn $2p_{3/2}$ (L_3) and $2p_{1/2}$ (L_2), respectively.[27] For RIXS, the values given in Sec. II for the resolution of the beamline and of the AERHA spectrometer were taken into account as a Gaussian broadening.

Within the plane lying perpendicular to the elongated axis, there are small Mn–O bond length differences (see Sec. I), which we neglect in the following analysis, i.e., we simply assume that the distortion lowers the symmetry of the Mn local environment from O_h to D_{4h}. The atomic matrix elements are branched[28–30] from the spherical symmetry corresponding to the atomic situation to the D_{4h} symmetry relevant to the local environment of the atom involved in the process. Writing the in-plane and the out-of-plane Mn–O distances as $a^\star$ and $b^\star$, respectively, the CF acting on Mn sites can be parametrized using Dq, Ds, and Dt as follows:[31] $Dq(u) = (1/6)ze\overline{r^4}/u^5$ ($u = a^\star$ or $b^\star$), $Ds = Cp(a^\star) - Cp(b^\star)$, where $Cp(u) = (2/7)ze\overline{r^2}/u^3$, and $Dt = (4/7)[Dq(a^\star) - Dq(b^\star)]$. Here, ze represents the charge of the ligand and $\overline{r^n}$ is the mean n^{th} power of the electron radial distribution of the $3d$ transition-metal ion. These parameters are related to the CF parameters used by Butler[25,28] as: $Dq = [1/(6\sqrt{30})]X_{400} - [7/(30\sqrt{42})]X_{420}$, $Ds = -(1/\sqrt{70})X_{220}$, and $Dt = -[2/(5\sqrt{42})]\,X_{420}$.

In the XAS simulations (see below the comparison with the experiment), the orientation of the electric vector of the linearly polarized light relative to the tilts of the C_4 axis of the MnO_6 octahedra is fully taken into account. State-of-the-art RIXS calculations were performed to obtain the isotropic response of the system. The implementation of anisotropic aspects in RIXS calculations is presently under development.[32] We note, however, that the CF parameters extracted from our simulations are reliable because the *energies* of the Mn d–d excitations are determined by the local D_{4h} symmetry of the Mn^{3+} ions, whatever the orientation of the octahedra to which they belong.

IV. EXPERIMENTAL AND COMPUTATIONAL RESULTS

The Mn $L_{3,2}$ XAS spectra of $TbMnO_3$ recorded at room temperature are shown in Fig. 2. According to the orientation of the crystallographic axes relative to the sample position [see Fig. 1(c)], at normal incidence, linear horizontal (LH) and linear vertical (LV) polarizations correspond to ($\mathbf{q}_{in} \perp \mathbf{a}, \mathbf{E} \parallel \mathbf{b}, \mathbf{q}_{in} \parallel \mathbf{c}$) and ($\mathbf{E} \parallel \mathbf{a}, \mathbf{q}_{in} \perp \mathbf{b}, \mathbf{q}_{in} \parallel \mathbf{c}$), respectively, where $\mathbf{q}_{in}$ is the wave vector of the incident beam with electric field $\mathbf{E}$. When the sample surface is oriented to 25° grazing incidence, the use of LH polarization delivers a configuration close to ($\mathbf{q}_{in} \perp \mathbf{a}, \mathbf{q}_{in} \parallel \mathbf{b}, \mathbf{E} \parallel \mathbf{c}$), while for LV polarization, the orientation can be described as ($\mathbf{E} \parallel \mathbf{a}, \mathbf{q}_{in} \parallel \mathbf{b}, \mathbf{q}_{in} \perp \mathbf{c}$). As these measurements were made in TEY mode, they are expected to be sensitive to the quality of the surface. It is seen that the spectra are hardly affected by the change in incidence angle of the incoming light indicating that contribution from surface contamination is negligible. This reinforces the reliability of far less surface sensitive RIXS data as compared to TEY. At low temperatures (≈25 K), the sample conductivity is substantially reduced, thus preventing measurements using the sample drain current.

All XAS spectra display a pronounced shoulder (denoted by a in Fig. 2) initiating a white line with three well-resolved maxima (b, c, and d) followed by a shoulder (e). Our spectra show only very slight polarization dependence, at variance with XAS TEY data previously reported for a single crystal[33] or thin films[34] with the same composition. However, our data are in excellent agreement with more recent XAS spectra.[35]

Mn L_3 RIXS spectra were recorded, with incoming LH polarized light (π polarization), at room temperature and at 25 K for all incoming photon energies $h\nu_{in}$ defined in Fig. 2. As the data show very similar spectral features for both temperatures, only the 25 K data are presented in Fig. 3. The main features indicated with dashed lines in Fig. 3 correspond to energy loss values of 1.6, 2.4, and 3.0 eV. As they appear at constant ($h\nu_{in} - h\nu_{out}$), we attribute them to *on-site* Mn d–d excitations. Broader features are also observed at higher energy, e.g., between ≈4 and 10 eV in the RIXS spectrum recorded at $h\nu_{in} = 640.0$ eV (see a in Fig. 2). As the energy loss associated with these features increases in the same way as the incoming photon energy, they are related either to CT excitations corresponding to $3d^4 \rightarrow 3d^5\underline{L}^{-1}$, where $\underline{L}$ denotes an oxygen ligand around the Mn site, or to fluorescence (or a combination of both).[36]

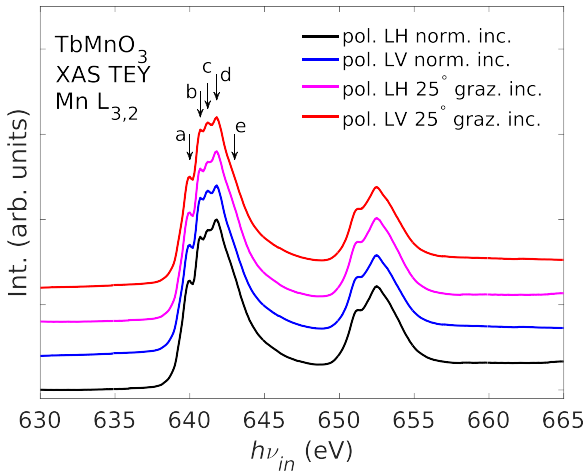

FIG. 2. Mn $L_{3,2}$ XAS for $TbMnO_3$ recorded at room temperature with photons having linear horizontal (LH) and linear vertical (LV) polarizations, as well as in two geometries: at normal incidence and 25° grazing incidence of the beam relative to the sample surface.

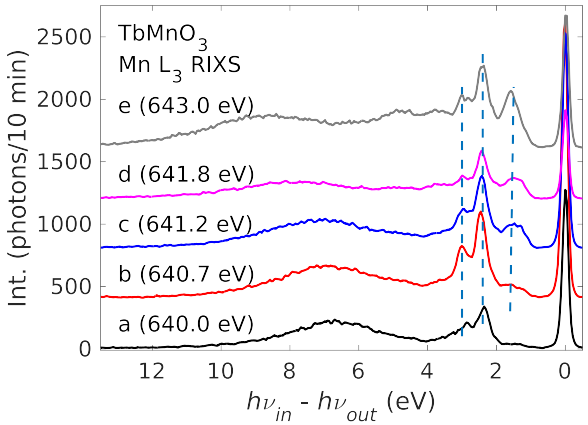

FIG. 3. Mn L_3 RIXS for $TbMnO_3$ recorded at 25 K. The letters refer to the Mn $L_{3,2}$ XAS spectrum (Fig. 2) and indicate the incident photon energies used in the RIXS measurements. The abscissa is given as the energy ($h\nu_{in} - h\nu_{out}$) lost by the photons in the inelastic scattering process. Vertical dashed lines are guide to the eye for the main groups of losses.

It is interesting to note that optical spectroscopy of the parent rare-earth manganites has outlined the difficulty of classifying these compounds either as CT or as Mott–Hubbard insulators[37] and has revealed the presence of an inter-site (Mn 3*d*–Mn' 3*d*) excitation.[38] RIXS measurements at the Mn *K* edge, obtained with an overall energy resolution of ~ 1 eV, have shown a broad energy-loss feature at ≈ 2.9 eV that has been interpreted on the basis of first principles band structure calculations to a mixture of on-site (Mn 3*d*–Mn 3*d*) and inter-site (Mn 3*d*–Mn' 3*d*) excitations.[39] Considering only on-site *d*–*d* excitations delivers an adequate interpretation of the Mn L_3 RIXS measurements in the present contribution.

Because of the overlap between Mn 3*d* states and O 2*p* ligand states, we expect to observe the signature of Mn *d*–*d* excitations when performing RIXS measurements at the O *K* resonance. This possibility was first identified in $CuGeO_3$[40] and confirmed in the case of NiO[41,42] and La_2CuO_4.[43] Our O *K* XAS and RIXS results for $TbMnO_3$ are presented in Fig. 4 (as before, the O *K* RIXS data recorded at room temperature and at 25 K have similar shape and only the low temperature data are shown in this figure). The XAS spectrum probes unoccupied O 2*p* states and displays four main structures for incident photon energies $h\nu_{in}$ of 529.4, 530.2, 533.6, and 535.8 eV. The RIXS spectra show two separable contributions. For incoming photon energies $528.4 \leq h\nu_{in} \leq 530.2$ eV, a Raman-like spectral feature is found at 2.4 eV constant energy-loss. Based on the Mn L_3 RIXS, it is attributed to a Mn *d*–*d* excitation by analogy with what has been reported in previous O *K* RIXS studies.[40–43] A second contribution arises from the resonant $2p \rightarrow 1s$ fluorescence-like emission (shown as vertical bars in the bottom panel of Fig. 4), at constant $h\nu_{out}$ photon energies, coming from the occupied O 2*p* density of states (DOS). The latter contribution sets in already when the incoming photon energy is tuned 1 eV below the first white line. The spectral weight of the resonant emission increases with the energy of the incoming photons and largely dominates the RIXS spectra, as expected. We note that the Raman-like contribution showing up at 2.4 eV energy loss can be conveniently disentangled, provided that a sufficient number of incident energies are used for recording the RIXS spectra.

In order to obtain a parametric description of the CF acting on the Mn^{3+} sites, we simulated the Mn $L_{3,2}$ XAS spectrum and the Mn L_3 RIXS spectra using the same set of *Dq*, *Ds*, and *Dt* values. The simulated spectra are shown in Fig. 5 along with the experimental results (for XAS, the case of LH polarized light at normal incidence is shown). We worked with a Racah parameter $B = 800\ \mathrm{cm}^{-1}$, given by *ab initio* Hartree–Fock calculations after reduction of the Slater–Condon parameters (see Sec. III). The best *Dq*, *Ds*, and *Dt* set was obtained after examination of a large number of combinations, as described in Ref. 44. As CT was not included in the calculations, we privileged agreement between predicted and experimental peak positions for RIXS and the main maxima of the L_3 XAS shape. The values obtained were as follows: $10Dq = 1.6$ eV, $Ds = 0.31$ eV, and $Dt = 0.06$ eV. Conserving these values for the core-hole state assumes that the presence of the core-hole potential does

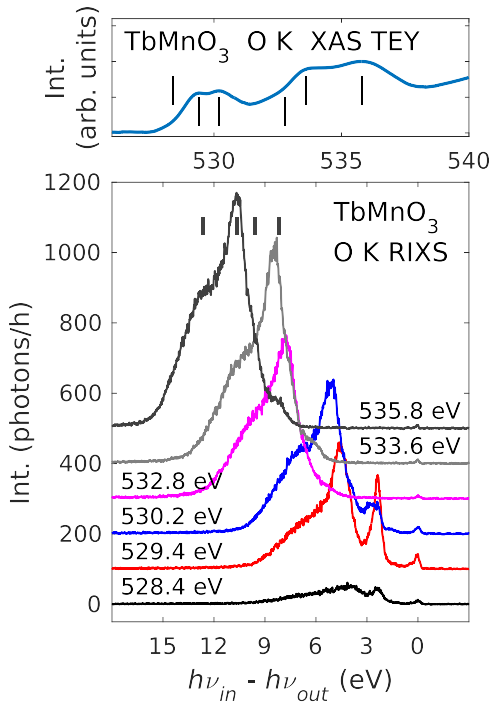

FIG. 4. XAS (top panel) and RIXS spectra (bottom panel) recorded for $TbMnO_3$ at O *K* edge. Vertical lines in the XAS spectrum (taken at room temperature) indicate the incoming photon energies used to record the RIXS spectra recorded at 25 K, the values being listed in the bottom panel. Short vertical bars in the lower panel are a guide to the eye for the main fluorescence-like bands recorded with $h\nu_{in} = 535.8$ eV.

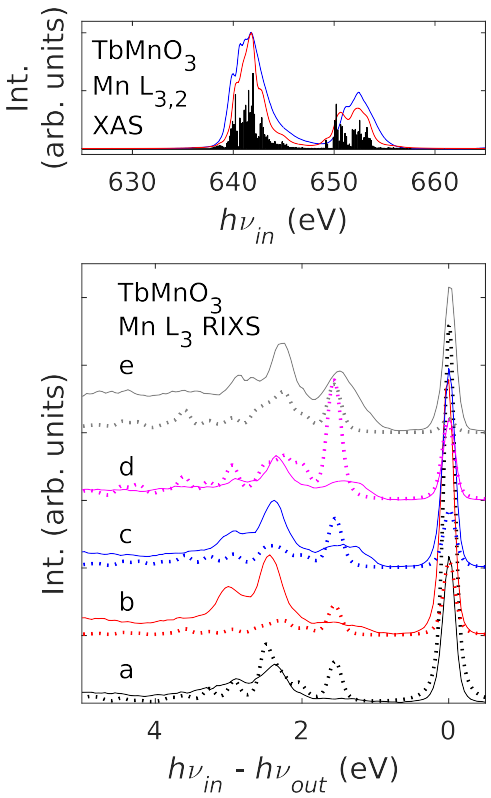

FIG. 5. Simulated and measured XAS and RIXS spectra of $TbMnO_3$ at Mn $L_{3,2}$ edges. Top panel: XAS (the non-resonant contribution has been subtracted to make the comparison with the simulation easier). XAS measured and calculated spectra are shown for LH incoming light at normal incidence. Bottom panel: the energies a–e used to record the RIXS spectra are the same as in Fig. 2; the continuous and dashed lines are the experimental and calculated spectra, respectively.

not alter the CF strength. This assumption, widely used in previous studies,[25] makes it possible to work with a reasonable number of CF parameters. The simulated results are in very good agreement with the measured spectra and allow, according to Ref. 44, the following identifications to be made: the peak located at 1.6 eV energy loss is due to transitions from the $^5B_{1g}$ ground state to a manifold of $^5A_{1g}+^5B_{2g}+^3E_g$ excited states; the peak at 2.4 eV and that at 3.0 eV can be attributed to $^5B_{1g}\rightarrow{}^5E_g+^3A_{1g}+^3A_{2g}+^1A_{1g}$ and $^5B_{1g}\rightarrow{}^3B_{1g}+^1B_{1g}+^3E_g+^3B_{2g}$ orbital excitations, respectively.

V. DISCUSSION

The CF approach has generally demonstrated its ability to provide a good understanding of the energy levels of 3*d* and 4*f* cations in a symmetrical environment of anions. However, the quantitative agreement of the theoretical predictions (point charge model, angular overlap model) with experiments is poor, even when covalent bonding is included within the framework of the ligand field theory. The main difficulties in the calculation of CF parameters arise from the moments $\overline{r^2}$ and $\overline{r^4}$ of the radial distribution. Typically, the experimental $\overline{r^2}/\overline{r^4}$ ratio is several times lower than the values calculated for free 3*d* ions (see Ref. 45 and references therein). A further complication is added by the way the ligands are described; the spatial extension of the O 2*p* states makes it difficult to handle the ligand in terms of point charges with an effective charge *ze* (see, e.g., Ref. 31) and demands for a more sophisticated approach. Efforts to take into account both electrostatic and hybridization effects continue to be made to get better predictions, as they are essential for a quantitative modelization of ferroelectric materials. Such a goal requires an accurate determination of phenomenological CF parameters.[46]

Some insight into the effect of CF on the unoccupied electronic states can be obtained from the O *K* edge spectra (Fig. 4). Electric dipole $1s\leftrightarrow 2p$ transitions bring out the unoccupied O 2*p* partial DOS in the XAS data as well as the occupied DOS in the fluorescence-like contribution to the RIXS data. Following the analysis of various Mn compounds where the transition metal is found in a distorted octahedral environment,[47–51] the O *K* XAS feature at 529.4 eV can be tentatively assigned to O 2*p* states hybridized with Mn $(3z^2-r^2)$ from the e_g branch and the 530.2 eV energy loss can be linked to O 2*p* states hybridized mainly with Mn (x^2-y^2) states. The energy separation $\Delta=0.8$ eV measured in O *K* XAS is expected to be different from $\Delta_{e_g}=\varepsilon_{(x^2-y^2)}-\varepsilon_{(3z^2-r^2)}$. The difference $\delta=\Delta-\Delta_{e_g}$ can be explained by the core-hole binding energy difference for oxygen atoms situated in-plane (planar positions) and out-of-plane (apical positions along the C_4 symmetry axis). According to the present parametrization, $\Delta_{e_g}=4Ds+5Dt=1.54$ eV, therefore leading to an anomalous core-hole binding energy difference $\delta\approx-0.74$ eV. This observation clearly indicates that such simple models to extract the CF splitting from the O *K* XAS can be applied to manganites only in particular cases. The hybridization between occupied O 2*p* and Mn 3*d* states can be observed from the O *K* fluorescence-like resonant emission: the spectra show four main bands, marked with short vertical bars in the RIXS spectra of Fig. 4. The relative intensity of the bands has a strong $h\nu_{in}$ dependence. The O 2*p* partial DOS calculations presented in Ref. 33 display a relatively good agreement with the unoccupied O 2*p* states obtained with the present O *K* XAS. On the other hand, agreement between occupied O 2*p* states revealed by O *K* resonant emission and calculations in Ref. 33 is rather poor.

Our approach involving the Mn L_3 edge relies only on symmetry considerations and provides an explicit way for characterizing the tetragonal distortion of MnO_6 octahedra in $TbMnO_3$. The CF parameters are the best values matching the D_{4h} environment. In other words, the parameters *Dq*, *Ds*, and *Dt* can be used without the need for renormalization accounting for the surrounding of the Mn^{3+} ion and are to be regarded as pure numerical parameters, including both symmetry effects and Mn 3*d*–O 2*p* hybridization. Recently, an attempt to better understand the contributions of electrostatic and hybridization effects has been presented,[52] based on Wannier functions. In particular, the $TbMO_3$ series, where M is a 3*d* transition-metal ion with a formal number n_d of *d* electrons, was studied; an hypothetical tetragonally distorted perovskite structure (space group *P*4/*mmm*; $a=3.86$ Å and $c/a=1.1$) was assumed whatever M. For $n_d=4$ (M = Mn), it is predicted that the hybridization should lead to an inversion of the energy levels corresponding to the (*xy*) and (*xz*, *yz*) states that originate from the octahedral t_{2g} state, i.e., the energy difference $\Delta_{t_{2g}}=\varepsilon_{(xy)}-\varepsilon_{(xz,yz)}$ was found negative in Ref. 52. The energy separation Δ_{e_g} between the (x^2-y^2) and $(3z^2-r^2)$ states remains positive in the model as expected from simple electrostatic considerations based on the shape of the *d* orbitals. This is not supported by our findings. Within the (*Ds*, *Dt*) parametrization, the energy differences are given by (see, e.g., Ref. 31): $\Delta_{t_{2g}}=3Ds-5Dt$ and $\Delta_{e_g}=4Ds+5Dt$. These expressions, derived from symmetry considerations, adopt a pure numerical parametrization, as already mentioned. According to our results, it is found that $\Delta_{t_{2g}}=0.63\,\text{eV}\,(>0)$ and $\Delta_{e_g}=1.54\,\text{eV}\,(>0)$. We note that the parameters obtained here lead to a separation of only 0.06 eV between the (*xy*) state from the t_{2g} branch and the $(3z^2-r^2)$ state from the e_g branch, clearly opening the possibility for state mixture. The magnitude of the Jahn–Teller splitting (>300 meV) of the Mn^{3+} 3*d* levels supports the dominant role attributed to Jahn–Teller effects in the orbital ordering in $TbMnO_3$.[12]

VI. CONCLUSIONS

Combining element specific RIXS and XAS measurements at the Mn $L_{3,2}$ edges with CF multiplet calculations provides accurate parameters for the description of tetragonal distortion of the Mn^{3+} environment in $TbMnO_3$. The present work represents a first step toward reliable calculations of the energies involved in ionic displacements which might enter the emergence of electric polarization in $TbMnO_3$ and are relevant to the description of the magnetic interactions in this compound.

ACKNOWLEDGMENTS

The authors thank R. Gaudemer for technical assistance. S.G.C., R.D., and J.-M.M. acknowledge the support of the

Agence Nationale de la Recherche (ANR), under Grant No. ANR-05-NANO-074 (HR-RXRS). Additional funding was provided by Synchrotron SOLEIL and UPMC. R.S. and H.D.Z. thank the support from NSF-DMR through Award No. DMR-1350002.

[1]D. I. Khomskii, *Transition Metal Compounds* (Cambridge University Press, Cambridge, 2014).
[2]S. Picozzi and C. Ederer, J. Phys.: Condens. Matter **21**, 303201 (2009).
[3]D. Khomskii, Physics **2**, 20 (2009).
[4]T. Kimura, T. Goto, H. Shintani, K. Ishizaka, T. Arima, and Y. Tokura, Nature **426**, 55 (2003).
[5]M. Kenzelmann, A. B. Harris, S. Jonas, C. Broholm, J. Schefer, S. B. Kim, C. L. Zhang, S.-W. Cheong, O. P. Vajk, and J. W. Lynn, Phys. Rev. Lett. **95**, 087206 (2005).
[6]T. Kimura, Annu. Rev. Mater. Res. **37**, 387 (2007).
[7]H. Katsura, N. Nagaosa, and A. V. Balatsky, Phys. Rev. Lett. **95**, 057205 (2005).
[8]M. Mostovoy, Phys. Rev. Lett. **96**, 067601 (2006).
[9]S. B. Wilkins, T. R. Forrest, T. A. W. Beale, S. R. Bland, H. C. Walker, D. Mannix, F. Yakhou, D. Prabhakaran, A. T. Boothroyd, J. P. Hill, P. D. Hatton, and D. F. McMorrow, Phys. Rev. Lett. **103**, 207602 (2009).
[10]H. C. Walker, F. Fabrizi, L. Paolasini, F. de Bergevin, J. Herrero-Martin, A. T. Boothroyd, D. Prabhakaran, and D. F. McMorrow, Science **333**, 1273 (2011).
[11]H. C. Walker, F. Fabrizi, L. Paolasini, F. de Bergevin, D. Prabhakaran, A. T. Boothroyd, and D. F. McMorrow, Phys. Rev. B **88**, 214415 (2013).
[12]A. Flesch, G. Zhang, E. Koch, and E. Pavarini, Phys. Rev. B **85**, 035124 (2012).
[13]X.-Y. Chen, L.-J. Chen, X.-B. Yang, Y.-J. Zhao, H.-C. Ding, and C.-G. Duan, J. Appl. Phys. **111**, 013901 (2012).
[14]A.-M. Haghiri-Gosnet and J.-P. Renard, J. Phys. D: Appl. Phys. **36**, R127 (2003).
[15]N. Hollmann, Z. Hu, T. Willers, L. Bohatý, P. Becker, A. Tanaka, H. H. Hsieh, H.-J. Lin, C. T. Chen, and L. H. Tjeng, Phys. Rev. B **82**, 184429 (2010).
[16]Y. Tokura and Y. Tomioka, J. Magn. Magn. Mater. **200**, 1 (1999).
[17]M. E. Bolívar Guarín, A. d M. Moreira, and N. Speziali, J. Appl. Cryst. **46**, 644 (2013).
[18]R. Kajimoto, H. Yoshizawa, H. Shintani, T. Kimura, and Y. Tokura, Phys. Rev. B **70**, 012401 (2004).
[19]L. J. P. Ament, M. van Veenendaal, T. P. Devereaux, J. P. Hill, and J. van den Brink, Rev. Mod. Phys. **83**, 705 (2011).
[20]T. Zou, Z. Dun, H. Cao, M. Zhu, H. Zhou, and X. Ke, J. Appl. Phys. **116**, 104101 (2014).
[21]M. Sacchi, N. Jaouen, H. Popescu, R. Gaudemer, J.-M. Tonnerre, S. G. Chiuzbăian, C. F. Hague, A. Delmotte, J. M. Dubuisson, G. Cauchon, B. Lagarde, and F. Polack, J. Phys.: Conf. Ser. **425**, 072018 (2013).
[22]S. G. Chiuzbăian, C. F. Hague, A. Avila, R. Delaunay, N. Jaouen, M. Sacchi, F. Polack, M. Thomasset, B. Lagarde, A. Nicolaou, S. Brignolo, C. Baumier, J. Lüning, and J.-M. Mariot, Rev. Sci. Instrum. **85**, 043108 (2014).
[23]R. D. Cowan, *The Theory of Atomic Spectra and Structure*, Los Alamos Series in Basic and Applied Sciences Vol. 3 (University of California Press, Berkeley, 1981).
[24]B. T. Thole, G. van der Laan, and P. H. Butler, Chem. Phys. Lett. **149**, 295 (1988).
[25]F. de Groot and A. Kotani, *Core Level Spectroscopy of Solids*, Advances in Condensed Matter Science (CRC Press, Boca Raton, FL, 2008).
[26]H. Ikeno, F. M. F. de Groot, E. Stavitski, and I. Tanaka, J. Phys.: Condens. Matter **21**, 104208 (2009).
[27]"Core-hole lifetime broadenings," in *Unoccupied Electronic States*, Topics in Applied Physics Vol. 69, edited by J. C. Fuggle and J. E. Inglesfield (Springer Verlag, Berlin, Heidelberg, New York, 1992), p. 347, Appendix B.
[28]P. H. Butler, *Point Group Symmetry, Applications, Methods and Tables* (Plenum Press, New York, 1981).
[29]B. G. Searle and P. H. Butler, J. Phys. A: Math. Gen. **21**, 1977 (1988).
[30]H. J. Ross, L. F. McAven, K. Shinagawa, and P. H. Butler, J. Comput. Phys. **128**, 331 (1996).
[31]B. N. Figgis and M. A. Hitchman, *Ligand Field Theory and Its Applications*, Special Topics in Inorganic Chemistry (Wiley-VCH, New York, 2000).
[32]A. Juhin, C. Brouder, and F. Groot, Cent. Eur. J. Phys. **12**, 323 (2014).
[33]J. M. Chen, J. M. Lee, C. K. Chen, T. L. Chou, K. T. Lu, S. C. Haw, K. S. Liang, C. T. Chen, H. T. Jeng, S. W. Huang, T. J. Yang, C. C. Shen, R. S. Liu, J. Y. Lin, and Z. Hu, Appl. Phys. Lett. **94**, 044105 (2009).
[34]K. H. Wu, I. C. Gou, C. W. Luo, T. M. Uen, J.-Y. Lin, J. Y. Juang, C. K. Chen, J. M. Lee, and J. M. Chen, Thin Solid Films **518**, 2275 (2010).
[35]H. Jang, J.-S. Lee, K.-T. Ko, W.-S. Noh, T. Y. Koo, J.-Y. Kim, K.-B. Lee, J.-H. Park, C. L. Zhang, S. B. Kim, and S.-W. Cheong, Phys. Rev. Lett. **106**, 047203 (2011).
[36]G. Ghiringhelli, M. Matsubara, C. Dallera, F. Fracassi, R. Gusmeroli, A. Piazzalunga, A. Tagliaferri, N. B. Brookes, A. Kotani, and L. Braicovich, J. Phys.: Condens. Matter **17**, 5397 (2005).
[37]A. S. Moskvin, A. A. Makhnev, L. V. Nomerovannaya, N. N. Loshkareva, and A. M. Balbashov, Phys. Rev. B **82**, 035106 (2010).
[38]M. W. Kim, S. J. Moon, J. H. Jung, J. Yu, S. Parashar, P. Murugavel, J. H. Lee, and T. W. Noh, Phys. Rev. Lett. **96**, 247205 (2006).
[39]J. M. Chen, J. M. Lee, S. W. Huang, K. T. Lu, H. T. Jeng, C. K. Chen, S. C. Haw, T. L. Chou, S. A. Chen, N. Hiraoka, H. Ishii, K. D. Tsuei, and T. J. Yang, Phys. Rev. B **82**, 094442 (2010).
[40]L.-C. Duda, J. Downes, C. McGuinness, T. Schmitt, A. Augustsson, K. E. Smith, G. Dhalenne, and A. Revcolevschi, Phys. Rev. B **61**, 4186 (2000).
[41]L.-C. Duda, T. Schmitt, M. Magnuson, J. Forsberg, A. Olsson, J. Nordgren, K. Okada, and A. Kotani, Phys. Rev. Lett. **96**, 067402 (2006).
[42]K. Okada and A. Kotani, J. Phys. Soc. Jpn. **72**, 797 (2003).
[43]V. Bisogni, L. Simonelli, L. J. P. Ament, F. Forte, M. Moretti Sala, M. Minola, S. Huotari, J. van den Brink, G. Ghiringhelli, N. B. Brookes, and L. Braicovich, Phys. Rev. B **85**, 214527 (2012).
[44]E. König and S. Kremer, *Ligand Field Energy Diagrams* (Springer Science+Business Media, New York, 2013), p. 179.
[45]M. Pollet and A. Artemenko, J. Phys. Chem. A **117**, 6536 (2013).
[46]N. M. Avram and M. G. Brik, *Optical Properties of 3d-Ions in Crystals: Spectroscopy and Crystal Field Analysis* (Tsinghua University Press and Springer-Verlag, Beijing, Berlin, 2013).
[47]J.-H. Park, C. T. Chen, S.-W. Cheong, W. Bao, G. Meigs, V. Chakarian, and Y. U. Idzerda, Phys. Rev. Lett. **76**, 4215 (1996).
[48]J.-H. Park, T. Kimura, and Y. Tokura, Phys. Rev. B **58**, R13330 (1998).
[49]M. Merz, P. Reutler, B. Büchner, D. Arena, J. Dvorak, Y. U. Idzerda, S. Tokumitsu, and S. Schuppler, Eur. Phys. J. B **51**, 315 (2006).
[50]V. Capogrosso, M. Malvestuto, I. P. Handayani, P. H. M. van Loosdrecht, A. A. Nugroho, E. Magnano, and F. Parmigiani, Phys. Rev. B **87**, 155118 (2013).
[51]R. U. Chandrasena, W. Yang, Q. Lei, M. U. Delgado-Jaime, K. D. Wijesekara, M. Golalikhani, B. A. Davidson, E. Arenholz, K. Kobayashi, M. Kobata, F. M. F. de Groot, U. Aschauer, N. A. Spaldin, X. Xi, and A. X. Gray, Nano Lett. **17**, 794 (2017).
[52]A. Scaramucci, J. Ammann, N. A. Spaldin, and C. Ederer, J. Phys.: Condens. Matter **27**, 175503 (2015).